J|A|C|S
ARTICLES
Published on Web 08/06/2002

Supramolecular Assembly at Interfaces: Formation of an Extended Two-Dimensional Coordinate Covalent Square Grid Network at the Air−Water Interface

Jeffrey T. Culp,[†] Ju-Hyun Park,[‡] Diktys Stratakis,[‡] Mark W. Meisel,[‡] and Daniel R. Talham*,[†]

Contribution from the Department of Chemistry, University of Florida, Gainesville, Florida 32611-7200, and Department of Physics and Center for Condensed Matter Sciences, University of Florida, Gainesville, Florida 32611-8440

Received March 25, 2002

Abstract: Reaction of a Langmuir monolayer of an amphiphilic pentacyanoferrate(3+) complex with Ni^{2+} ions from the subphase results in the formation of a two-dimensional iron−nickel cyanide-bridged network at the air−water interface. The network can be transferred to various supports to form monolayer or multilayer lamellar films by the Langmuir−Blodgett (LB) technique. The same network does not form from homogeneous reaction conditions. Therefore, the results demonstrate the potential utility of an interface as a structure director in the assembly of low dimensional coordinate covalent network solids. Characterization of the LB film extended networks by X-ray photoelectron spectroscopy (XPS), FT-IR spectroscopy, SQUID magnetometry, X-ray absorption fine structure (XAFS), and grazing incidence synchrotron X-ray diffraction (GIXD) revealed a face-centered square grid structure with an average domain size of 3600 $Å^2$. Magnetic measurements indicated that the network undergoes a transition to a ferromagnetic state below a T_c of 8 K.

Introduction

Many advances in the pursuit of nanoscale objects make use of supramolecular assembly, the synthesis of larger structures from molecular building blocks.[1] Inspired by biological self-assembly, much supramolecular chemistry holds structures together with directed, noncovalent interactions such as hydrogen bonding, van der Waals, electrostatic, and π-stacking forces.[1,2] However, bonding is not restricted to weak interactions, and the directional properties of coordinate covalent bonding have also led to many interesting structures.[3−12]

Among the motivations for the pursuit of nanometer scale objects[13,14] is the need for electronics architectures that are beyond the scope of present-day lithographic technologies. Such architectures will require both nanometer scale device components and infrastructures such as wires, insulation, and shielding that can service or interface with these devices at the nanometer scale.[2] In addition to electronics and information storage, other applications of nanoscale architectures include catalysis and separations, while nanoscale objects also have tremendous potential as molecular level probes and transducers for chemical recognition sensing.[14]

Many of these applications are likely to require positioning the structures at surfaces. For example, the electronics architectures mentioned above will have to be fabricated onto a support. Two-dimensional (2D) grid structures have been proposed as separations media,[15−18] which will require their positioning at an interface between phases. Interfaces may also play a role in the "manufacture" of supramolecular structures, providing a way of directing interactions by orienting molecules at the surface for subsequent reaction. Therefore, there is a

* To whom correspondence should be addressed. E-mail: talham@chem.ufl.edu.
[†] Department of Chemistry.
[‡] Department of Physics and Center for Condensed Matter Sciences.

(1) *Comprehensive Supramolecular Chemistry;* Lehn, J. M., Atwood, J. L., Davies, J. E. D., McNicol, D. D., Vogtle, V., Eds.; Pergamon Press: Oxford, U.K., 1996.
(2) Philip, D.; Stoddart, J. F. *Angew. Chem., Int. Ed. Engl.* **1996**, *25*, 1154.
(3) Fredericks, J. R.; Hamilton, A. D. In *Supermolecular Control of Structure and Reactivity;* Hamilton, A. D., Ed.; John Wiley and Sons: New York, 1996; p 1.
(4) Baxter, P. N. W. In *Comprehensive Supramolecular Chemistry*; Sauvage, J. P., Hosseini, M. W., Eds.; Pergamon Press: Oxford, U.K., 1996; Vol. 9, p 165.
(5) Fujita, M. In *Comprehensive Supramolecular Chemistry;* Sauvage, J. P., Hosseini, M. W., Eds.; Pergamon Press: Oxford, U.K., 1996; Vol. 9, p 253.
(6) Funeriu, D. P.; Lehn, J.-M.; Baum, G.; Fenske, D. *Chem. Eur. J.* **1997**, *3*, 99.
(7) Vance, A. L.; Alcock, N. W.; Busch, D. H.; Heppert, J. A. *Inorg. Chem.* **1997**, *36*, 5132.
(8) Yaghi, O. M.; Li, H.; Davis, C.; Richardson, D.; Groy, T. L. *Acc. Chem. Res.* **1998**, *31*, 474.
(9) Yaghi, O. M.; Li, H.; Groy, T. L. *Inorg. Chem.* **1997**, *36*, 4292.
(10) Lopez, S.; Kahraman, M.; Harmata, M.; Keller, S. W. *Inorg. Chem.* **1997**, *36*, 6138.
(11) Lu, J.; Paliwala, T.; Lim, S. C.; Yu, C.; Niu, T.; Jacobson, A. J. *Inorg. Chem.* **1997**, *36*, 923.
(12) Dunbar, K. R.; Heintz, R. A. *Prog. Inorg. Chem.* **1997**, *45*, 283.
(13) Ozin, G. A. *Adv. Mater.* **1992**, *4*, 612.
(14) Morales, A. M.; M. Lieber, C. *Science* **1998**, *279*, 208.
(15) Harrison, R. M.; Brotin, T.; Noll, B. C.; Michl, J. *Organometallics* **1997**, *16*, 3401.
(16) Magnera, T. F.; Peslherbe, L. M.; Korblova, E.; Michl, J. *J. Organomet. Chem.* **1997**, *548*, 83.
(17) Pospisil, L.; Heyrovsky, M.; Pecka, J.; Michl, J. *Langmuir* **1997**, *13*, 6294.
(18) Magnera, T. F.; Pecka, J.; Vacek, J.; Michl, J. *Nanostructured Materials*; American Chemical Society: Washington, D.C., 1997; p 213.

significant need to investigate the application of supramolecular assembly processes at interfaces.[19−27] With a growing understanding of how to synthesize supramolecular objects, we can now begin to study how the requirements of such assembly processes can be adapted for fabrication at interfaces. Included in this goal is the need to investigate ways to use the interface itself as a structure-directing feature in the assembly of supramolecular architectures.

Air−liquid interfaces are often used to direct assembly processes, and a careful understanding of these processes is now possible largely as a result of surface sensitive characterization methods, including grazing incidence X-ray diffraction.[28] Traditional Langmuir monolayers can form two-dimensional molecular crystals[28−31] or can selectively bind molecules or ions from the subphase to produce multicomponent assemblies.[28,32−34] Langmuir monolayers are also used to induce the heterogeneous nucleation of three-dimensional crystals, where chemical or stereochemical features of the monolayer can direct the morphology, orientation, or chemical identity of the product crystals.[35−38] Supramolecular objects have also been prepared in situ at the air−water interface.[28] For example, the 2×2 and 3×3 metal ion molecular grids first described by Lehn et al.[39−41] have been formed at the air−water interface by reaction of Langmuir monolayers of the linear multidentate ligands with aqueous metal ions.[24,25] These and other examples are included in a recent comprehensive review by Kuzmenko et al.[28] Less common are extended two-dimensional covalent grid networks. The best-described examples are those of Michl and co-workers who use the principles of modular chemistry to prepare surface-anchored two-dimensional covalent networks.[16,18,42−45]

Scheme 1. Assembly of a Two-Dimensional Square Grid Network at the Air−Water Interface

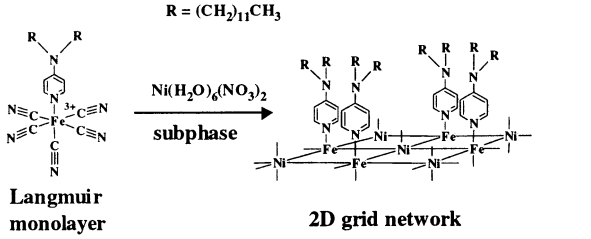

As part of our investigation of these issues, this paper describes the assembly of a two-dimensional nickel−iron cyanide grid network at the air−water interface. Numerous solid-state compounds based on bridging cyanides are known[46−56] with the prototype being Prussian blue. Recent interest in these compounds stems from the cyanide ligand's ability to efficiently mediate magnetic exchange, and many new mixed-metal Prussian blue-like structures have been developed with fascinating magnetic properties.[46−49,57,58] Structures with one- and two-dimensional coordinate covalent networks are also known,[49−52] and metal cyanide complexes have been used as building blocks in the preparation of "zero-dimensional" clusters.[53−56] In all cases, the structure-directing elements are the well-defined bond angles of the transition metal complexes and the linear bridging cyanide ligands.

Our approach for assembly at an interface is outlined in Scheme 1. The target is a square grid nickel−iron cyanide network that arises from the 90° bond angles around the starting iron cyanide complex. The product is a single monolayer of a two-dimensional square grid because the amphiphilic dialkylaminopyridine ligand confines the iron complex to the interface, which then directs the condensation reaction within the plane of the water surface. In the absence of the interface, the pentacyanoferrate(3+) starting complex is capable of forming bridges that lead to geometries other than a square grid, and when the reaction is carried out in solution, only amorphous products are observed. The interface facilitates bridging in the equatorial plane of the amphiphilic complex and therefore plays an important role in controlling the final structure.

(19) Shipway, A.; Willner, I. *Acc. Chem. Res.* **2001**, *34*, 421.
(20) Armand, F.; Albouy, P.; Cruz, F.; Normand, M.; Huc, V.; Goron, E. *Langmuir* **2001**, *17*, 3431.
(21) Bowden, N.; Terfort, A.; Carbeck, J.; Whitesides, G. M. *Science* **1997**, *276*, 233.
(22) Bowden, N.; Choi, I. S.; Grzybowski, B. A.; Whitesides, G. M. *J. Am. Chem. Soc.* **1999**, *121*, 5375.
(23) Bowden, N.; Arias, F.; Deng, T.; Whitesides, G. M. *Langmuir* **2001**, *17*, 1757.
(24) Weissbuch, I.; Baxter, P. N. W.; Cohen, S.; Cohen, H.; Jaer, K. K.; Howes, P. B.; Als-Nielsen, J.; Hanan, G. S.; Schubert, U. S.; Lehn, J.-M.; Leiserowitz, L.; Lahav, M. *J. Am. Chem. Soc.* **1998**, *120*, 4850.
(25) Weissbuch, I.; Baxter, P. N. W.; Kuzmenko, I.; Cohen, H.; Cohen, S.; Kjaer, K.; Howes, P. B.; Als-Nielsen, J.; Lehn, J. M.; Leiserowitz, L.; Lahav, M. *Chem. Eur. J.* **2000**, *6*, 725.
(26) Mingotaud, C.; Lafuente, C.; Amiell, J.; Delhaes, P. *Langmuir* **1999**, *15*, 289.
(27) Huo, Q.; Russell, K. C.; LeBlanc, R. M. *Langmuir* **1998**, *14*, 2174.
(28) Kuzmenko, I.; Rapaport, H.; Kjaer, K.; Als-Nielsen, J.; Weissbuch, I.; Lahav, M.; Leiserowitz, L. *Chem. Rev.* **2001**, *101*, 1659.
(29) Ulman, A. *An Introduction to Ultrathin Organic Films: From Langmuir−Blodgett to Self-Assembly*; Academic Press: Boston, MA, 1991.
(30) Jacquemain, D.; Wolf, S. G.; Leveiller, F.; Deutsch, M.; Kjaer, K.; Als-Nielsen, J.; Lahav, M.; Leiserowitz, L. *Angew. Chem., Int. Ed. Engl.* **1992**, *31*, 130.
(31) Kaganer, V.; Möhwald, H.; Dutta, P. *Rev. Mod. Phys.* **1999**, *71*, 779.
(32) Leveiller, F.; Bohm, C.; Jacquemain, D.; Mohwald, H.; Leiserowitz, L.; Kjaer, K.; Als-Nielsen, J. *Langmuir* **1994**, *10*, 819.
(33) Weissbuch, I.; Guo, S.; Edgar, R.; Cohen, S.; Howes, P.; Kjaer, K.; Als-Nielsen, J.; Lahav, M.; Leiserowitz, L. *Adv. Mater.* **1998**, *10*, 117.
(34) Hensel, V.; Godt, A.; Popovitz-Biro, R.; Cohen, H.; Jensen, T. R.; Kjaer, K.; Weissbuch, I.; Lifshitz, E.; Lahav, M. *Chem. Eur. J.* **2002**, *8*, 1413.
(35) Landau, E. M.; Levanon, M.; Leiserowitz, L.; Lahav, M.; Sagiv, J. *Nature* **1985**, *318*, 353.
(36) Frostman, L. M.; Ward, M. D. *Langmuir* **1997**, *13*, 330.
(37) Mann, S.; Heywood, B. R.; Rajam, S.; Walker, J. B. A.; Davey, R. J.; Birchall, J. D. *Adv. Mater.* **1990**, *2*, 257.
(38) Whipps, S.; Khan, S. R.; O'Palko, F. J.; Backov, R.; Talham, D. R. *J. Cryst. Growth* **1998**, *192*, 243.
(39) Hanan, G. S.; Volkmer, D.; Schubert, U. S.; Lehn, J. M.; Baum, G.; Fenske, D. *Angew. Chem., Int. Ed. Engl.* **1997**, *36*, 1842.
(40) Baxter, P. N. W.; Lehn, J. M.; Kneisel, B. O.; Fenske, D. *Angew. Chem., Int. Ed. Engl.* **1997**, *36*, 1978.
(41) Baxter, P. N. W.; Lehn, J. M.; Fischer, J.; Youinou, M. T. *Angew. Chem., Int. Ed. Engl.* **1994**, *33*, 2284.
(42) Michl, J.; Magnera, T. F. *Proc. Natl. Acad. Sci. U.S.A.* **2002**, *99*, 4788.
(43) Varaksa, N.; Pospíil, L.; Magnera, T. F.; Michl, J. *Proc. Natl. Acad. Sci. U.S.A.* **2002**, *99*, 5012.
(44) Magnera, T. F.; Michl, J. *Atual. Fís. Quim. Org.* **1998**, 50.
(45) Harrison, R. M.; Magnera, T. F.; Vacek, J.; Michl, J. In *Towards Designer Solids*; Michl, J., Ed.; Kluwer: Dordrecht, The Netherlands, 1997; pp 1−16.
(46) Gadet, V.; Mallah, T.; Castro, I.; Verdaguer, M. *J. Am. Chem. Soc.* **1992**, *114*, 9213.
(47) Mallah, T.; Thiebaut, S.; Verdaguer, M.; Veillet, P. *Science* **1993**, *262*, 1554.
(48) Ferlay, S.; Mallah, T.; Ouahes, R.; Veillet, P.; Verdaguer, M. *Nature* **1995**, *378*, 701.
(49) Ohba, M.; Fukita, N.; Okawa, H. *J. Chem. Soc., Dalton Trans.* **1997**, *10*, 1733.
(50) Re, N.; Gallo, E.; Floriani, C.; Miyasaka, H.; Matsumoto, N. *Inorg. Chem.* **1996**, *35*, 6004.
(51) Miyasaka, H.; Matsumoto, N.; Kawa, H.; Re, N.; Gallo, E.; Floriani, C. *J. Am. Chem. Soc.* **1996**, *118*, 981.
(52) Ohba, M.; Okawa, H.; Fukita, N.; Hashimoto, Y. *J. Am. Chem. Soc.* **1997**, *119*, 1011.
(53) Zhong, Z. J.; Seino, H.; Mizobe, Y.; Hidai, M.; Fujishima, A.; Ohkoshi, S.; Hashimoto, K. *J. Am. Chem. Soc.* **2000**, *122*, 2952.
(54) Berseth, P. A.; Sokol, J. J.; Shores, M. P.; Heinrich, J. L.; Long, J. R. *J. Am. Chem. Soc.* **2000**, *122*, 9655.
(55) Larionova, J.; Gross, M.; Pilkington, M.; Andres, H.; Stoeckli-Evans, H.; Gudel, H. U.; Decurtins, S. *Angew. Chem., Int. Ed.* **2000**, *39*, 1605.
(56) Rogez, G.; Parsons, S.; Paulsen, C.; Villar, V.; Mallah, T. *Inorg. Chem.* **2001**, *40*, 3836.
(57) Hatlevik, O.; Buschmann, W. E.; Zhang, J.; Manson, J. L.; Miller, J. S. *Adv. Mater.* **1999**, *11*, 914.
(58) Holmes, S. M.; Girolami, G. S. *J. Am. Chem. Soc.* **1999**, *121*, 5593.

A potential obstacle to confining reactants to an interface is that reactivity can be limited by restricted diffusion.[17] A gas−liquid interface minimizes this problem, allowing studies to focus on the structure-directing elements of the reactants and surface. In addition, structures formed at the air−water interface can be transferred from the water surface to solid supports using standard Langmuir−Blodgett film methods. The transferred films allow for more thorough measurement of the structural and physical properties of the interface-formed networks. The condensation reaction outlined in Scheme 1 is followed at the air−water interface with surface pressure measurements and with Brewster angle microscopy (BAM), and the structure of the resulting nickel−iron cyanide network is confirmed in transferred films with optical and infrared spectroscopy, X-ray absorption fine structure (XAFS), grazing incidence X-ray diffraction (GIXD), and magnetization measurements.

Experimental Section

Synthesis. (a) Materials. Unless otherwise indicated, all reagents were purchased from Aldrich (Milwaukee, WI) or Fisher Scientific (Pittsburgh, PA) and used without further purification. The 4-aminopyridine was recrystallized from water prior to use.

(b) Instrumentation. All NMR spectra were obtained on a Varian VXR-300 spectrometer. The characteristic solvent peaks were used as reference values. Elemental analyses and mass spectrometry analyses were performed by the University of Florida Spectroscopic Services laboratory, where high-resolution mass spectra were collected on a MAT 95Q, Finnigan MAT (San Jose, CA). Melting points were obtained on a Thomas-Hoover capillary melting point apparatus and are uncorrected. UV−vis spectra were obtained on a Hewlett-Packard 8452A diode array spectrophotometer. IR spectra as KBr pellets were recorded on a Mattson Instruments (Madison, WI) Research Series-1 FTIR spectrometer with a deuterated triglycine sulfate (DTGS) detector.

(c) *N*-Methyl-4-(didodecylamino)pyridinium iodide (1). A solution of 3.54 g (0.015 mol) of *N*-methyl-4-aminopyridinium iodide[59] and 9.37 g (0.0375 mol) of 1-bromododecane in acetonitrile (75 mL) was refluxed over 5.5 g of K_2CO_3 (0.04 mol) for 3 days. The acetonitrile was removed and the organic materials dissolved in chloroform and filtered. The chloroform was removed under reduced pressure, and 20 mL of diethyl ether was added to the orange oil that remained. Addition of the ether solution to 150 mL of pentane with vigorous stirring precipitated the product. The solid was filtered and washed well with diethyl ether and dried under vacuum (7.8 g, 91%) ^{1}H NMR (CD_3Cl, ppm): δ 8.45, d, 2H; 6.79, d, 2H; 4.11, s, 3H; 3.37, t, 4H; 1.54, m, 4H; 1.19−1.25, m, 36H; 0.80, t, 6H. Anal. Calcd for $C_{30}H_{57}N_2I$: C, 62.92; H, 10.03; N, 4.89. Found: C, 63.25; H, 10.64; N, 4.89. Mp: 99−101 °C. MS (445).

(d) 4-(Didodecylamino)pyridine (2). Demethylation of **1** was accomplished in a manner analogous to a previously reported procedure for the demethylation of pyridinium salts.[60] A stirred mixture of 7.5 g of **1** and 40 g of pyridine hydrochloride were refluxed under nitrogen in the absence of solvent. After 24 h the mixture was cooled and 75 mL of water was added to dissolve the excess pyridine hydrochloride. The crude product was filtered off and redissolved in 100 mL of chloroform. The chloroform solution was extracted three times with 50 mL portions of concentrated ammonium hydroxide and dried over anhydrous $MgSO_4$ before removal of the solvent under reduced pressure. Acetonitrile (100 mL) was added to the oil that remained, and the mixture was vigorously stirred in an ice bath. The precipitated solid was redisolved in diethyl ether (100 mL), treated with 200 mg of activated carbon, and filtered through Celite. The ether filtrate was mixed with 80 mL of acetonitrile and concentrated under a stream of N_2 to precipitate the pure product as beige solid. The solid was washed with acetonitrile and dried under vacuum (3.9 g, 70%). ^{1}H NMR (CD_3Cl, ppm): δ 8.16, d, 2H; 6.41, d, 2H; 3.25, t, 4H; 1.57, m, 4H; 1.26−1.31, m, 36H; 0.88, t, 6H. Anal. Calcd for $C_{29}H_{54}N_2$: C, 80.86; H, 12.64; N, 6.50. Found: C, 81.14; H, 12.28; N, 6.58. Mp: 54−56 °C MS (431 ($+H^+$)).

(e) Bis(tetramethylammonium)pentacyano(4-(didodecylamino)-pyridine)ferrate(III)·6H$_2$0 (3). The preparation of the amphiphilic pentacyanoferrate complex was adapted from a previously reported procedure for the preparation of disodium pentacyano(4-(octadecylamino)pyridine)ferrate(III).[61] To a solution of 1.9 g (0.0044 mol) of **2** in methanol (50 mL) at 40 °C was added 0.40 g (0.0015 mol) of $Na_3[Fe(CN)_5NH_3]\cdot xH_2O$. The suspension was stirred for 12 h in air yielding a dark purple solution. The methanol was concentrated at room temperature under reduced pressure to a volume of 10 mL and 40 mL of chloroform added. The insoluble iron salts were filtered off through Celite and the solvents removed. The product was dissolved in 50 mL of methanol and precipitated by the addition of $AgBF_4$ (0.003 mol) in 25 mL of methanol. The solid was filtered, washed with methanol and ether, and transferred to a methanol solution of tetramethylammonium bromide (0.003 mol). The mixture was stirred vigorously for 4 h and then filtered to remove the AgBr. The violet filtrate was concentrated at room temperature to a few milliliters and added to 75 mL of acetonitrile. Concentration of the acetonitrile under a stream of nitrogen, followed by the addition of several volumes of acetone, precipitated the complex as a violet powder, which turns blue upon hydration. The solid was dried under vacuum in a desiccator over P_2O_5 (0.412 g, 35%). IR (KBr pellet, cm^{-1}): ν_{C-N} 2126, 2116. Anal. Calcd for $C_{42}H_{90}N_9O_6Fe$: C, 57.78; H, 10.4; N, 14.44. Found: C, 57.30; H, 10.76; N, 14.68.

Films. (a) Materials. Unless noted, all reagents were used as received.

(b) Substrate Preparation. Single-crystal (100) silicon wafers, purchased from Semiconductor Processing Co. (Boston, MA), were used as deposition substrates for X-ray photoelectron spectroscopy (XPS). X-ray diffraction, FT-IR, UV−vis, and GIXD samples were prepared on petrographic slides that were purchased from Buehler Ltd (Lake Bluff, IL). Samples for SQUID and XAFS investigations were prepared on Mylar (Dupont) substrates cleaned prior to use with absolute ethanol. The silicon, glass, and quartz substrates were cleaned using the RCA procedure[62] and dried under nitrogen. All substrate surfaces were made hydrophobic by deposition of a monolayer of OTS.[63,64]

(c) Instrumentation. The LB films were prepared by using a KSV Instruments 5000 trough modified to operate with double barriers. The surface pressure was measured with a filter paper Wilhelmy plate suspended from a KSV microbalance. Subphase solutions were prepared from 17.8 to 18.1 MΩ cm water delivered with a Barnstead Epure system. The XPS spectra were obtained on a Perkin-Elmer (Eden Prairie, MN) PHI 5000 series spectrometer using the Mg Kα line source at 1253.6 eV. Typical operating pressure was 4×10^{-10} bar. X-ray diffraction was performed with a Philips APD 3720 X-ray powder diffractometer with the Cu Kα line, $\lambda = 1.54$ Å. Magnetization measurements were performed on a Quantum Design MPMS SQUID magnetometer.

GIXD and XAFS experiments using synchrotron radiation were performed at the Advanced Photon Source, Argonne, IL, at the Materials Research Collaborative Access Team beam line (sector 10). The XAFS spectra of LB films transferred to Mylar were recorded in fluorescence mode using a Lytle detector. The sample film was oriented at 45° to the incident beam and the detector at 90° relative to the incident beam. Energy calibration was accomplished by simultaneously recording

(59) Posiomek, E. J. *J. Org. Chem.* **1963**, *28*, 590.
(60) Ruiz, A.; Rocca, P.; Marsais, F.; Godard, A.; Quéguiner, G. *Tetrahedron Lett.* **1997**, *38*, 6205.
(61) Armand, F.; Sakaragi, H.; Tokumaru, K. *New J. Chem.* **1993**, *17*, 351.
(62) Kern, W. *J. Electrochem. Soc.* **1990**, *137*, 1887.
(63) Maoz, R.; Sagiv, J. *J. Colloid Interface Sci.* **1984**, *100*, 465.
(64) Netzer, L.; Sagiv, J. *J. Am. Chem. Soc.* **1983**, *105*, 674.

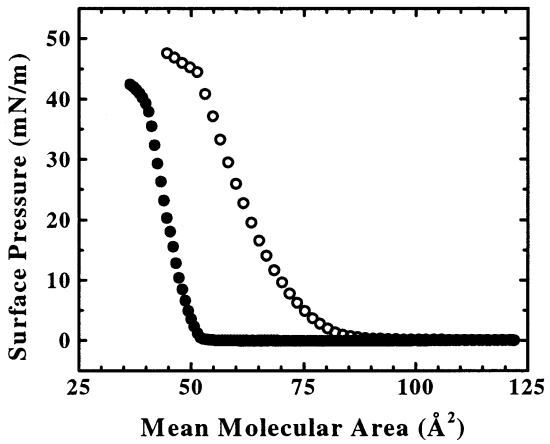

Figure 1. Room temperature surface pressure vs mean molecular area isotherms for complex **3** over 10^{-3} M NaCl (open circles) and over a 1 g/L $Ni(NO_3)_2$ (filled circles).

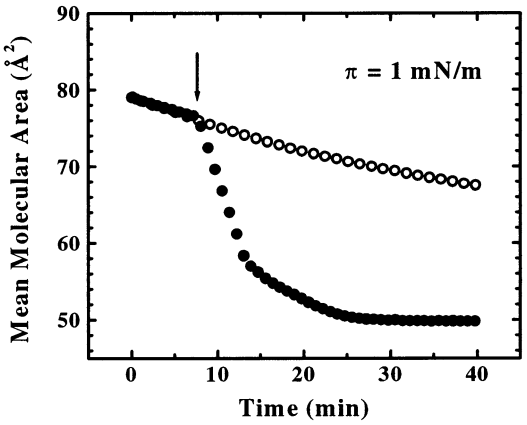

Figure 2. Change in mean molecular area versus time at a surface pressure (π) of 1 mN/m for complex **3** over NaCl (open circles) and over NaCl with subsequent injection of a $Ni(NO_3)_2$ solution (at the time indicated by the arrow) under the monolayer (filled circles). Condensation of the monolayer occurs immediately after injection of the Ni^{2+} solution.

transmission XAFS spectra through the appropriate metal foil positioned behind the LB film sample. Transmission intensity was measured using an ion chamber detector charged with the appropriate air−N_2 ratio to give a linear response over the scanned energy range. The sample used for XAFS was 100 bilayers. XAFS scans were taken over both the Fe and Ni edges from 150 eV before the edge step to 1 keV beyond the edge in separate runs for each edge. Data analysis was performed using the Winxas program.[65] Background subtraction and normalization to the edge step was done with a linear fit to the preedge region and a second-order fit to the postedge region. The atomic absorption correction was done on the k^3-weighted data using a cubic spline function. Fourier transforms of the k^3-weighted data were done in combination with a Bessel window function. No smoothing functions or Fourier filters were applied to the data. The GIXD scans were performed on LB films transferred to glass slides. The sample was positioned in the center of an eight-circle Huber goniometer and oriented at an angle of 0.13° relative to the incident beam. The incident beam was collimated to 200 μm high by 1500 μm wide and tuned to a wavelength of 1.254 Å. Diffracted intensity in the *xy* plane was measured using a NaI scintillation counter mounted on the Huber goniometer. The diffracted signal was collimated prior to the detector using Soller slits giving an experimental resolution on the order of 0.015 $Å^{-1}$.

(d) Film Preparation. The amphiphilic iron complex **3** was spread onto the water surface from a chloroform solution. All multilayer films of the nickel−iron cyanide network were transferred as Y-type films onto hydrophobic substrates at a surface pressure of 25 mN/m over a subphase of 1 g/L $Ni(NO_3)_2$ at ambient temperature. The average transfer ratios for both the upstroke and downstroke were 0.85.

Results

Langmuir Monolayers and LB Film Transfer. The amphiphilic iron complex **3** forms a well-behaved monolayer on the water surface (10^{-3} M NaCl). Brewster angle microscopy indicates the amphiphile is in a liquid expanded state at zero surface pressure at room temperature. Compression of the monolayer at room temperature produces the surface pressure versus area isotherm shown in Figure 1. The complex is slightly soluble on water and a creep of approximately 15 $Å^2$/molecule/h is seen at a surface pressure of 1 mN/m, Figure 2.

The behavior of **3** over a subphase containing Ni^{2+} is markedly different from that with Na^+. Brewster angle microscopy indicates that the monolayer is in a condensed phase at zero surface pressure when the subphase contains Ni^{2+}. Evidence for a condensed phase at zero surface pressure is also given by the isotherm shown in Figure 1. The mean molecular area of 52 $Å^2$ at the onset of pressure for the complex over a Ni^{2+} subphase is nearly identical to the mean molecular area at collapse of the complex over Na^+. Additionally, the slope of the isotherm is steeper when **3** is compressed over a Ni^{2+} subphase. As will be demonstrated, this behavior results from a condensation reaction between the ferric amphiphile and the aqueous nickel ions.

The reaction at the air−water interface was also detected by monitoring the change in mean molecular area (MMA) versus time at a constant surface pressure as shown in Figure 2. A monolayer of **3** was first compressed over aqueous NaCl to a pressure of 1 mN/m. A slow and linear creep is seen in the film due to the slight solubility of **3**. When 10 mL of a solution of $Ni(NO_3)_2 \cdot 6H_2O$ (at a concentration to give a final subphase concentration of 1 mM Ni^{2+}) is then injected under the monolayer, a rapid drop in the MMA is seen. The MMA eventually stabilizes at a value of 50 $Å^2$, which after correction for the initial creep of ca. 2−3 $Å^2$, agrees well with the 52 $Å^2$ seen at 1 mN/m in the compression isotherm performed over Ni^{2+}, shown in Figure 2.

To further characterize the product of the condensation reaction occurring on the water surface, the networks were transferred to various supports by the Langmuir−Blodgett technique. The nickel−iron cyanide network transferred well as Y-type films from a subphase containing 1 g/L $Ni(NO_3)_2$ at a surface pressure of 25 mN/m giving an average transfer ratio of 85% (due to the rigid nature of the film) on both the up strokes and the down strokes on all substrates used. In contrast, in the absence of Ni^{2+}, amphiphile **3** transfers on the down stroke, but washes off on the up stroke.

Spectroscopic Analyses. Pentacyanoferrate(III) complexes coordinated to a 4-aminopyridine ligand display an intense ligand to metal charge-transfer band between 500 and 700 nm, depending on the identity of the 4-aminopyridine derivative and the nature of the solvent.[66,67] This charge-transfer band is also observed in the transferred films containing the nickel−iron

(65) Ressler, T. *J. Synchrotron. Radiat.* **1998**, *5*, 118.

(66) Hrepic, N. V.; Malin, J. M. *Inorg. Chem.* **1979**, *18*, 409.
(67) Armand, F.; Sakuragi, H.; Tokumaru, K. *J. Chem. Soc., Faraday Trans.* **1993**, *89*, 1021.

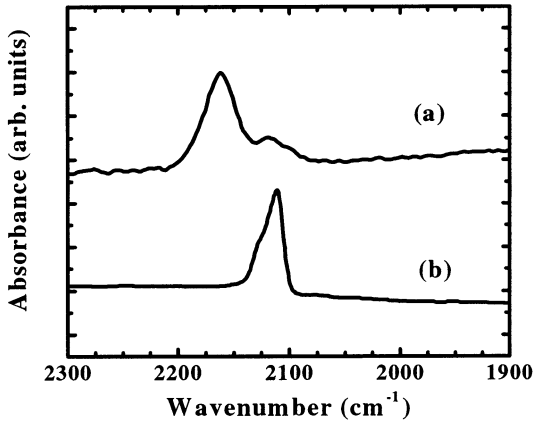

Figure 3. FT-IR absorption spectra of the C−N stretching region for (a) a monolayer film of the nickel−iron cyanide grid network transferred to a silicon ATR crystal and (b) a KBr pellet of pure **3**.

cyanide network. The intensity of the charge-transfer band increases linearly with the number of transferred bilayers and demonstrates a reproducible transfer of the network from one bilayer to the next. In addition, the presence of this band in the LB films confirms that the integrity of the iron complex is preserved over the course of film formation.

Evidence that nickel is incorporated in the transferred film is found by XPS. A survey scan of a monolayer transferred on the upstroke onto a clean silicon wafer shows both Fe ($2p_1$ and $2p_3$) and Ni ($2p_1$ and $2p_3$) peaks. Analysis of the integrated areas of the XPS multiplex scans using a takeoff angle of 80° and taking into account differences in photoelectron escape depths[68−70] for both sets of peaks yields an Fe:Ni ratio of 1:1 ± 10%. This ratio is expected if the Ni^{2+} ions are incorporated into a face-centered square grid assembly as depicted in Scheme 1.

Confirmation of cyanide bridging in the monolayer networks is found by comparing the C−N IR stretches in the LB film and a KBr pellet of pure **3** (Figure 3). In **3**, the cyanide-stretching region shows a strong band at 2111 cm^{-1} and a shoulder at 2126 cm^{-1}. These bands are in agreement with the pseudo C_{4v} symmetry of the complex. The FT-IR spectrum of a monolayer of **3** reacted with Ni^{2+} and transferred to a silicon ATR crystal shows a dominant cyanide stretching band at 2162 cm^{-1} and a weaker band at 2118 cm^{-1}. This shift to higher energy is typical when cyanide assumes a bridging mode.[71]

XAFS Analysis. The nonphase-shift corrected Fourier transforms of the k^3-weighted XAFS of the nickel−iron cyanide network transferred onto Mylar are shown in Figure 4 for the iron and nickel edges. Both sets of data show a similar pattern with three dominant peaks attributed to the first three coordination shells. For the iron edge, the first two peaks correspond to the C and N of the cyanide ligand, respectively, and the third peak to the nickel ion coordinated to the nitrogen end of the cyanide bridge. For the nickel edge transform, the peak assignments can be made with the first peak corresponding to the cyanide nitrogen and most likely coordinated water, the second peak to the cyanide carbon, and the third peak to the iron atom. The significant intensity of the peaks at approximately

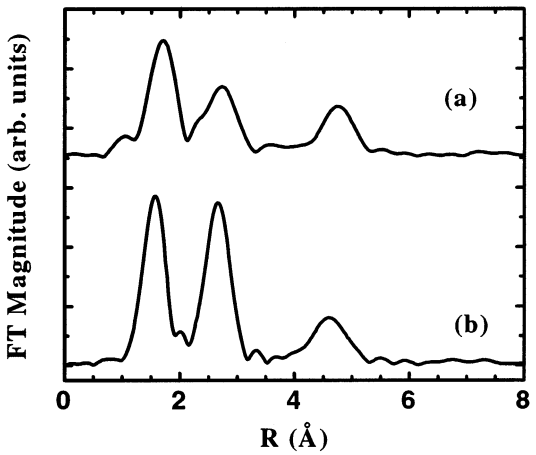

Figure 4. Magnitude of the Fourier transforms (FT) of the (a) nickel edge and (b) iron edge k^3-weighted XAFS for a 100 bilayer sample of the nickel−iron cyanide grid network transferred to Mylar. The *R* axis has not been corrected for phase shifts. No amplification factors were applied to either trace.

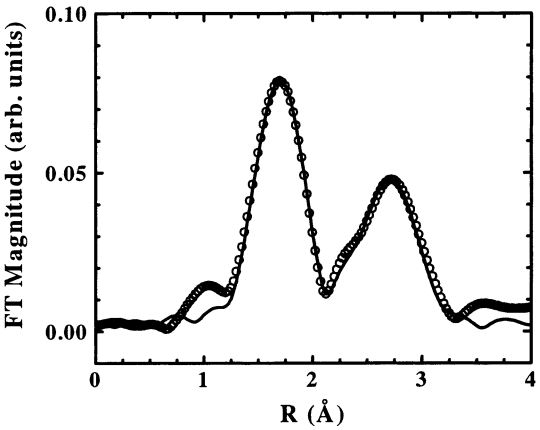

Figure 5. Fit (solid line) to the first two coordination shells of the Fourier transformed nickel edge XAFS (circles) of the nickel−iron cyanide grid network on Mylar. The fit was calculated using FEFF7 codes for a model Ni^{2+} cluster coordinated in-plane by the nitrogen end of four cyanides and axially by two oxygen ligands.

4.5 Å in both radial plots has been explained in other cyanide-bridged systems as resulting from the focusing effect of the linear cyanide bridge.[72,73]

The results of a fit to the first two coordination shells in the nickel edge k^3-weighted Fourier transformed XAFS data is shown in Figure 5. The fit was accomplished using the program Winxas with inputs from theoretical XAFS parameters generated from FEFF 7.0 codes[74,75] for a model nickel cluster composed of two axial oxygen atoms and four equatorial nitrogen-bound, iron-terminated cyanide ligands. The coordination number for Ni was fixed and both shells were fit simultaneously using an intrinsic reduction factor (S_0^2) of 0.52 for each and an edge energy shift (ΔE_0) of 1.0 and 6.0 for the first and second shells, respectively. The S_0^2 and ΔE_0 values used in the fit were similar in magnitude to those reported in the XAFS analysis of a similar metal-cyanide system.[76] The bond distances extracted from the

(68) Seah, M. P.; Dench, W. A. *Surf. Interface Anal.* **1979**, *1*, 1.
(69) Laibinis, P. E.; Bain, C. D.; Whitesides, G. M. *J. Phys. Chem.* **1991**, *95*, 7017.
(70) Brundle, C. R.; Hopster, H.; Swalen, J. D. *J. Chem. Phys.* **1979**, *70*, 5190.
(71) Zhan, S. Z.; Guo, D.; Zhang, X. Y.; Du, C. X.; Zhu, Y.; Yang, R. N. *Inorg. Chim. Acta* **2000**, *298*, 57.
(72) Giorgetti, M.; Berrettoni, M.; Filipponi, A.; Kulesza, P. J.; Marassi, R. *Chem. Phys. Lett.* **1997**, *275*, 108.
(73) Zhang, H. H.; Filipponi, A.; Di Cicco, A.; Scott, M. J.; Holm, R. H.; Hedman, B.; Hodgson, K. O. *J. Am. Chem. Soc.* **1997**, *119*, 2470.
(74) Zabinsky, S. I.; Rehr, J. J.; Ankudinov, A.; Albers, R. C.; Eller, M. J. *Phys. Rev. B* **1995**, *52*, 2995.
(75) Ankudinov, A. Ph.D. Thesis, University of Washington, 1996.

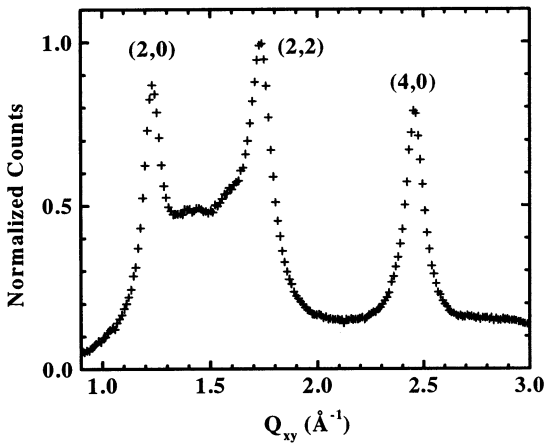

Figure 6. GIXD pattern obtained for a 39-bilayer sample of the nickel−iron cyanide grid network transferred to a glass slide. The peaks can be indexed to a face-centered square grid network with a cell edge of 10.2 Å.

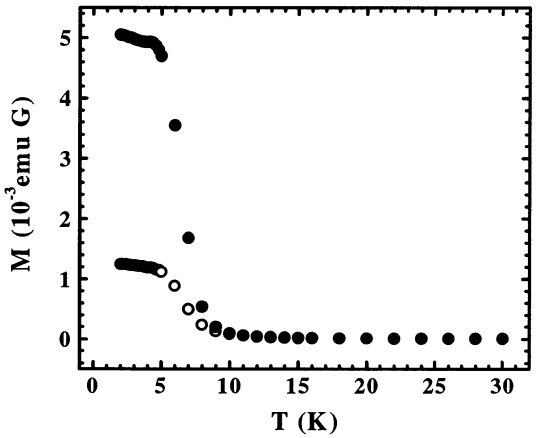

Figure 7. Temperature dependence of the magnetization after field cooling in 20 G with the sample surface aligned parallel (filled circles) and perpendicular (open circles), to the magnetic field. The measuring field was 20 G. The break at $T_c = 8$ K is indicative of long-range ferromagnetic order between the Fe^{3+} ($S = 1/2$) and Ni^{2+} ($S = 1$) centers.

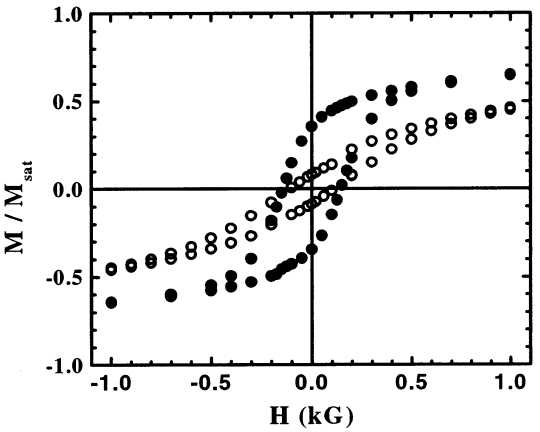

Figure 8. Hysteresis loops measured at 2 K with the sample surface aligned parallel to (filled circles) and perpendicular to (open circles) the applied magnetic field. The magnetization is normalized to the saturation magnetization.

fitting procedure were (in Å) Ni−N, 2.09; Ni−O, 2.11; Ni−C, 3.22; and C−N, 1.13; and are reasonable if compared to similar compounds.[52,77,78] Fits to the Ni edge XAFS were limited to the first two coordination shells due to complexities arising from the large number of multiple scattering pathways contributing to the third coordination shell.

X-ray Diffraction and GIXD. The lamellar order in the multilayer films of the nickel−iron cyanide network was confirmed by X-ray diffraction from a 30-bilayer sample. An intense diffraction peak at 2.5° 2θ and a weaker harmonic at 5° 2θ can be assigned to the (001) and (002) Bragg reflections and yield an inter-bilayer spacing of 35 Å. This inter-bilayer spacing is reasonable for the size of the amphiphile deposited as Y-type bilayers.

Grazing incidence X-ray diffraction was used to verify the presence of any long-range in-plane structural correlations in the film. The diffraction pattern obtained for a 39-bilayer sample of the iron-cyanide-nickel network transferred to glass is shown in Figure 6. The counts are normalized to the most intense peak and plotted versus the in-plane scattering vector $Q_{xy} = (4\pi/\lambda)(\sin \theta_{xy})$. The three intense peaks can be assigned to the (2,0), (2,2), and (4,0) Bragg reflections at d spacings of 5.10, 3.61, and 2.56 Å, respectively, from a face-centered square cell with an edge of $a = 10.2$ Å. The broad background centered at ca. $Q_{xy} = 1.41$ Å^{-1} and the shoulder at 1.58 Å^{-1} are likely due to the poorly organized alkyl chains.[31,79] The isolated (4,0) peak was fit to a Lorentzian function and yielded a full width at half-maximum ($Q_{xy_{fwhm}}$) of 0.1 Å^{-1}. Insertion of this value into the Scherrer equation,[80] $\xi = [(1.8\pi)/(Q_{xy_{fwhm}})]$, yields an average crystalline coherence length (ξ) of ∼60 Å, or 5 unit cell lengths, indicating that the 2D networks cover an average area of approximately 3600 Å^2.

Magnetic Properties. The magnetic properties of a 10 cm^2 sample containing 300 bilayers (150 bilayers/side) of the nickel−iron cyanide network transferred to Mylar were investigated by SQUID magnetometry. Two measurements were performed, one with the sample surface oriented parallel to the magnetic field and one with the sample surface oriented perpendicular to the magnetic field. The background-corrected field-cooled magnetization versus temperature plots obtained in a field of 20 G are shown in Figure 7.

The rise in magnetization below $T_c = 8$ K observed in both orientations is attributed to the onset of long-range ferromagnetic order. The magnetic behavior is clearly anisotropic, with the sample displaying a stronger magnetic response when the surface is oriented parallel to the magnetic field. The presence of a ferromagnetic state at low temperature is further supported by the magnetization vs field data taken at 2 K. The sample shows a rapid increase in magnetization at low field followed by a gradual approach toward saturation at higher fields. Cycling the magnetic field at 2 K results in the hysteresis loops (corrected for the diamagnetic background) shown in Figure 8. The plots are normalized to the magnetization at 5 T. Again, there is clear anisotropy in the magnetic behavior between the two orientations of the sample with respect to the field. When the field is parallel to the sample surface, the magnetization increases more rapidly with respect to the field and the remnant magnetization is 35% versus 8% in the perpendicular orientation. The coercive field

(76) Yokoyama, T.; Ohta, T.; Sato, O.; Hashimoto, K. *Phys. Rev. B* **1998**, *58*, 8257.
(77) Kou, H.; Bu, W.; Liao, D.; Jiang, Z.; Yan, S.; Fan, Y.; Wang, G. *J. Chem. Soc., Dalton Trans.* **1998**, 4161.
(78) Ohba, M.; Okawa, H.; Ito, T.; Ohto, A. *J. Chem. Soc., Chem. Commun.* **1995**, 1545.
(79) Als-Nielsen, J.; Jacquemain, D.; Kjaer, K.; Leveiller, F.; Lahav, M.; Leiserowitz, L. *Phys. Rep.* **1994**, *246*, 251.
(80) Guinier, A. *X-ray Diffraction*; Freeman: San Francisco, 1968.

is also slightly anisotropic, being 140 G in the parallel orientation and 110 G in the perpendicular orientation.

Discussion

Choice of System and Monolayer Behavior. Designing a system to result in the formation of a coordinate-covalent network at the air−water interface requires the appropriate transition metal complex building blocks. Octahedral transition metal ions possessing linear bridging ligands are well-suited to the assembly of square-grid networks since the required 90° bond angles are inherently present. By substituting one position with a hydrophobic ligand, the building block can be made amphiphilic and thus tailored for assembly reactions at the air−water interface. Condensation of the amphiphilic building block can then be accomplished by reaction with a suitable aqueous transition metal ion contained in the subphase. Confinement of the reacting system to the water surface directs the resulting structure to a two-dimensional motif.

The numerous examples of pentacyanoferrate complexes and the substitutional inertness of the cyanide ligand make this class of compounds well-suited to our assembly strategy. Multilayer films of the single chain derivative of **3**, (4-octadecylaminopyridine)pentacyanoferrate(III) (**4**) have previously been described.[81] The sodium salt of **4** was reported to be too soluble for film preparations, but when prepared as a mixed film with hexadecyltrimethylammonium counterions, stable Langmuir monolayers resulted. No difficulties with hydration of the single-chain complex were reported.

We decided to modify the pentacyanoferrate complex to the dual chain derivative to match more closely the size of the amphiphilic ligand with that of the metal complex headgroup. The addition of a second alkyl chain also decreased the solubility of the complex and eliminated the need for long-chain alkylammonium counterions. It was found to be beneficial, however, to exchange the sodium counterions for tetramethylammonium ions to decrease the hygroscopic nature of the complex and to aid its dissolution in chloroform. The resulting complex forms a Langmuir monolayer that creeps slowly on water (Figure 2) but forms a highly stable film after reaction with aqueous Ni^{2+} ions to form an insoluble polymeric network.

Evidence for the condensation reaction is seen in-situ at the air−water interface. In the absence of Ni^{2+}, **3** forms a liquid expanded phase upon compression. This behavior is reasonable, as amphiphiles with 12-carbon alkyl tails do not normally form condensed phases at the air−water interface at room temperature.[82] Upon addition of Ni^{2+}, a condensed phase is seen in the pressure vs area isotherm and in Brewster angle microscopy. The mean molecular area of 52 $Å^2$ at the onset of pressure correlates with the limiting area per molecule of the complex alone and suggests that the film is highly condensed at zero pressure over the Ni^{2+} subphase.

In a mixed-metal cyanide square grid network (Scheme 1), a centered unit cell will have two iron amphiphiles per unit cell. Doubling the area per molecule, determined from the pressure vs area isotherm, gives a cell area of 104 $Å^2$, which then corresponds to a cell edge distance of 10.2 Å. This value is in agreement with the 10.2 $Å^2$ determined for the cell edge by GIXD and suggests that the mean molecular area is determined by the lattice spacing of the inorganic two-dimensional grid network and not by the van der Waals interactions of the organic chains.

Furthermore, BAM and surface pressure data indicate that the nickel−iron cyanide network forms with or without preorganization of the monolayer. That is, the MMA obtained by compression of the iron amphiphile over a Ni^{2+} subphase is very close to the MMA obtained after injection of a Ni^{2+} solution under an organized monolayer of the iron complex. A condensed film is formed at zero pressure over the Ni^{2+} subphase, and subsequent compression of the film only acts to push together domains that have already assembled at the interface.

Structure of the Network. The formation of an extended two-dimensional array is dependent on the exclusive bridging of the four in-plane cyanide ligands, as bridging of the trans cyanide ligand would effectively terminate the structure and result in an amorphous inorganic polymer. Evidence for a well-organized network from GIXD, XAFS, and FT-IR suggests that while coordination of the axial cyanide is possible, this mode is most likely labile in the absence of the added stability brought on by extended bridging interactions.

The results of the GIXD clearly show the presence of a structurally coherent inorganic network in the mixed metal film. The three peaks shown in Figure 6 fit very well to the expected (*h*,*k*) pattern for a face-centered square grid network. The unit cell edge length of 10.2 Å deduced from the diffraction data is very similar to that reported in cubic Prussian blue derivatives.[83] The high background scattering near 1.4 and 1.6 $Å^{-1}$ is in the range of Q_{xy} normally seen for alkyl chain packing and suggests that the alkyl chains are loosely organized. This observation would be expected in light of the large area per alkyl chain in the condensed network.

The XAFS data complement the conclusions of the GIXD experiments. The Ni−N, C−N, and Ni−C distances of 2.09, 1.13, and 3.22 Å, respectively, were obtained from modeling the Ni edge XAFS. Combining these bond lengths with the average Fe−C bond length of 1.95 Å reported for other Fe−CN−Ni bridged systems,[52,77] leads to a Ni−Fe separation of 5.17 Å. This value is close to the 5.10 Å separation deduced from the GIXD. The quality of the XAFS fit supports the modeled nickel coordination environment in which the octahedral nickel ions are coordinated in-plane by the nitrogen terminus of the cyanide bridge and the axial sites by oxygen, most likely from coordinated water.

Magnetism. The formation of a structurally coherent inorganic network at the air−water interface is confirmed by the transition to a ferromagnetic state below 8 K in the multilayer film containing 150 bilayers per side. The ability of the cyanide ligand to mediate magnetic exchange between two paramagnetic metal ions is well-known and has been extensively explored in cubic Prussian blue derivatives. In particular, the Fe^{3+}/Ni^{2+} Prussian blue[84,85] was found to be ferromagnetic with a T_c of

(81) Armand, F.; Okada, S.; Yase, K.; Matsuda, H.; Nakanishi, H.; Sakuragi, H.; Tokumaru, K. *Jpn. J. Appl. Phys.* **1993**, *32*, 1186.
(82) Mingotaud, A.-F.; Mingotaud, C.; Patterson, L. K. *Handbook of Monolayers*, 1st ed.; Academic Press: London, 1993; Vol. 1.
(83) Ludi, A.; Gudel, H. U. *Struct. Bonding* **1973**, *14*, 1.
(84) Gadet, V.; Bujoli-Doeuff, M.; Force, L.; Verdaguer, M.; Makhi, E.; Deroy, A.; Besse, J. P.; Chappert, C.; Veillet, P.; Renard, J. P.; Beauvillain, P. In *Molecular Magnetic Materials, NATO ASI Series, Series E*; Gatteschi, J. D., Kahn, O., Miller, J. S., Palacio, F., Eds.; Kluwer: Dordrecht, The Netherlands, 1991; Vol. 198, p 281.
(85) Juszczyk, S.; Johansson, C.; Hanson, M.; Ratuszna, A.; Malecki, G. *J. Phys.: Condens. Matter.* **1994**, *6*, 5697.

23 K. In addition, ferromagnetic exchange has also been reported in a series of two-dimensional cyanide-bridged iron−nickel compounds with T_c's on the order of 10 K.[52,86] The ferromagnetic behavior of these materials is rationalized[87] by realizing that for octahedral metal centers, the magnetic orbitals are the Fe^{3+} ($S = 1/2$) t_{2g} and the Ni^{2+} ($S = 1$) e_g sets, and that the cyanide orbitals that overlap with each of them are orthogonal.

For the Fe^{3+}/Ni^{2+} LB film system, the ordering temperature of 8 K is lower than the T_c of 23 K observed in the cubic analogue and is more similar in magnitude to the ordering temperature reported in other low-dimensional Fe−CN−Ni networks.[88] Lower ordering temperatures for the 2D systems relative to the cubic analogues is expected as the number of exchange pathways per magnetic ion is reduced. Further evidence for a two-dimensional network is obtained from the anisotropic magnetic behavior seen in the film. The stronger magnetic response of the sample when oriented with the surface parallel to the magnetic field suggests a magnetic easy axis within the plane of the network. A strict analysis of a magnetic vector in the film is limited though due to uncertainties in how the microscopic surface roughness of the substrate affects variations in the orientation of network sheets relative to the plane defined by the macroscopic substrate. The high anisotropy of the magnetization, however, does discriminate against the magnetic behavior arising from cubic Prussian blue-like particles and is highly suggestive of a low-dimensional system.[89] More detailed studies on the magnetic properties of the LB film networks are ensuing since the unique structural features of these monolayer networks may provide experimental probes of the exchange coupling interactions in metal cyanide networks and how the issue of dimensionality influences ordering in mixed-spin 2D systems.[90,91]

Mechanism and Structure Directing Elements. The two-dimensional nickel−iron cyanide network forms at the air−water interface but does not require preorganization of the amphiphiles. The condensation reaction proceeds in the absence of applied surface pressure when the amphiphile **3** is spread on the Ni^{2+} containing subphase, in which case subsequent reduction of the surface area simply compresses the preformed domains. Compression of the film thus appears to do little to extend the in-plane order of the networks and instead, only works to increase the density of the domains allowing for better transfer of the networks to solid supports. Preorganization of the amphiphile, followed by injection of Ni^{2+} ions into the subphase results in the same network, with no significant difference in domain organization.

Control of the reaction to form the square grid network results from the orientational constraints of the octahedral metal complex with linear cyanide bridging in combination with the interface as a structure-directing element. This view is supported by attempts to form the same networks from solution. The analogous reaction of **3** with Ni^{2+} in methanol yields an insoluble precipitate, which is shown by X-ray diffraction to be amorphous. When compared to the homogeneous reaction, the air−water interface not only directs the structure of the final material but also acts to enhance the structural coherence length as well.

It is interesting to compare the mechanism of formation of the metal cyanide two-dimensional networks to other examples of Langmuir−Blodgett films that contain inorganic networks. For example, there are now several examples of metal phosphonate based LB films where the inorganic extended solid networks determine the in-plane structures.[92−94] The difference is that, for the metal phosphonates, the LB films form with the same structure that forms in the solid state. The structure is determined by the inorganic lattice energy. With the metal phosphonates, the LB film processing directs where the structure will form and affords control of the fabrication to one layer at a time, but the air−water interface does not act as a structure-directing element. In contrast, the iron cyanide−nickel network described here does not form from compound **3** in the absence of the interface. The interface directs where the reaction will take place and limits the reaction to one layer at a time, but, importantly, it also directs the structure.

Conclusions

An amphiphilic octahedral iron complex containing linear cyanide ligands was designed and synthesized as a building block for the assembly of two-dimensional square grid nickel−iron cyanide networks at the air−water interface. The reaction of Langmuir monolayers of this complex with aqueous nickel ions contained in the subphase results in the formation of coordinate covalent networks. Characterization of these networks by various techniques indicates that the structure is two-dimensional and coherent over an average domain size of 3600 $Å^2$. Magnetic measurements indicate a ferromagnetically ordered state below 8 K with the magnetic behavior highly dependent on the orientation of the sample with respect to the field. This synthetic method demonstrates that the air−water interface can function as a structure-directing element in the assembly of new supramolecular network solids and, in addition, provides a means for transferring these materials in a controlled fashion to solid supports. This assembly strategy may aid in the future development of nanoscale materials and with interfacing them at a surface.

Acknowledgment. During the course of this work we have benefited from conversations with O. A. Starykh of Hofstra University and G. R. Torres and P. Delhaes at the Centre de Recherche Paul Pascal. This research was supported by the National Science Foundation through Grant DMR-9900855 (D.R.T.) and by the American Chemical Society through Grant ACS-PRF-36163-AC5 (M.W.M., D.R.T.). Use of the Advanced Photon Source was supported by the U.S. Department of Energy, Office of Science, Office of Basic Energy Sciences, under Contract No. W-31-109-ENG-38. We also acknowledge support from the Materials Research Collaborative Access Team (MR-CAT) at the Advanced Photon Source.

JA026312E

(86) Fukita, N.; Ohba, M.; Okawa, H. *Mol. Cryst. Liq. Cryst.* **2000**, *342*, 217.
(87) Verdaguer, M.; Bleuzen, A.; Marvaud, V.; Vaissermann, J.; Seuleiman, M.; Desplanches, C.; Scuiller, A.; Train, C.; Garde, R.; Gelly, G.; Lomenech, C.; Rosenman, I.; Veillet, P.; Cartier, C.; Villain, F. *Coord. Chem. Rev.* **1999**, *192*, 1023.
(88) Ohba, M.; Okawa, H. *Coord. Chem. Rev.* **2000**, *198*, 313.
(89) Kahn, O.; Larionova, J.; Ouahab, L. *Chem. Commun.* **1999**, 945.
(90) Koga, A.; Kawakami, N. *J. Phys. Soc. Jpn.* **2000**, *69*, 1834.
(91) Takushima, Y.; Koga, A.; Kawakami, N. *Phys. Rev. B* **2000**, *61*, 15189.
(92) Seip, C. T.; Granroth, G. E.; Meisel, M. W.; Talham, D. R. *J. Am. Chem. Soc.* **1997**, *119*, 7084.
(93) Fanucci, G. E.; Talham, D. R. *Langmuir* **1999**, *15*, 3289.
(94) Petruska, M. A.; Talham, D. R. *Chem. Mater.* **1998**, *10*, 3673.